The influences of various auxetic cores on natural frequencies and forced vibration behavior of sandwich beam fabricated by 3D printer based on third -order shear deformation theory

Rohollah Hosseini [*], Masoud Babaei, Alireza Naddaf

Faculty of Mechanical and Mechatronics Engineering, Imam Hossein University, Tehran, Iran

Abstract

In this article, free and forced vibration analyses of 3D printed FG sandwich beam based on higher order beam theory is investigated. The core and face sheets of sandwich beam are integrally fabricated by 3D printer. Therefore, ignoring the delamination between face sheets and core is a correct assumption. Three different cells are considered for the core including Re-entrant auxetic cell, anti-tetrachiral auxetic cell and conventional honeycomb cell. These cells are arranged along the thickness of structure based on cell thickness in four various patterns. The effective mechanical properties of cells are estimated by analytical relations. Finite element methods and Lagrange equations are employed for obtaining the effective stiffness and mass matrices of the sandwich beam. Finally, the influences of various parameters including various types of cells, various patterns of cell along the thickness of structure, thickness coefficient, the geometry of cells such as the interior angle and dimensions of cells on natural frequencies and transient deflection of structure have been studied. The results denote that the arrangement of cells along the thickness plays an important role on the vibration response of structure. On the other hand, for uniform thickness distribution of cells, Re –entrant auxetic cell has higher natural frequencies than other cells while in FG arrangements of cells, anti-tetrachiral cell with pattern A has higher natural frequencies than Re-entrant auxetic cell.

Keywords: Free vibration; Forced vibration; FG graded auxetic cell; FEM; beam, higher order beam theory;

1. Introduction

Sandwich structures are widely used in many industries such as marine& submarine, aerospace, automobiles, etc. These structures are fabricated from two major part including face sheets and core. The face sheets are located at the bottom and top of the core. The face sheets are usually stronger than core and protect the core from external forces and environmental condition such as temperature and humidity. In these structures, the shapes, thickness and mechanical property of core plays an important role in behavior of them under static, dynamic loading. Due to there are a lot of investigations have been performed about the type of material, thickness and shapes of cores and face sheets subjected to various loading. Here, the articles are reviewed which are related to dynamic analysis of sandwich structures fabricated by 3D printer. In detailed, Gunasegeran and Sudhagar [1] employed numerical and experimental approach to investigate free and forced vibration behavior of 3D printed bioinspired sandwich beam made of PLA

---

[*] Corresponding Author Email: r.hosseini.mech@gmail.com (R.Hosseini)

based on higher order shear deformation theory (HSDT). Theoretical and experimental study on the vibration and dynamic response of a 3D-printed sandwich Beam with an Hourglass lattice truss core was resented by Guo et al. [2]. Rajpal et al. [3] investigated vibration behavior of 3D-printed polymer-based Magnetorheological elastomers (MR) sandwich beam under discretized magnetic field by employing experimental approach. Ghanadpour et al. [4] presented numerical and experimental solution for structural behavior and bending response of 3D-printed sandwich beams with strut-based lattice core. Li et al. [5] investigated the static and dynamic response of 3D-printed self-similar hierarchical honeycombs subjected to quasi-static and dynamic in-plane compression. Solyaev [6] utilized numerical and experimental methods to investigate the static and dynamic analyses of 3d-printed polyamide sandwich beams with different type of the lattice cores. An excellent agreement was governed between numerical and experimental results. Essassi et al. employed [7] applied experimental and numerical analysis to perform an investigation about dynamic behavior of a bio-based sandwich with an auxetic core. Sharif et al. [8] analyzed static and modal behavior of sandwich beam structure with magnetorheological honeycomb core. The core was made of PLA (Polylactic acid) and ABS (Acrylonitrile butadiene styrene) materials. Design and modelling of auxetic and hybrid honeycomb structures for in-plane property enhancement was presented by Ingrole, Hao and Liang. [9]. The new idea in this investigation was related to hybrid arrangement of cells. In reference [10], the authors applied experimental measurements and multiscale finite element method (MsFEM) for investigation the static bending and free vibrations of beams with four different mesostructures and two print orientations. Wu et al. [11] employed Bernoulli–Euler beam and Timoshenko beam hypothesis to investigate free vibration analysis and multi-objective optimization of lattice sandwich beams by employing non-dominated sorting genetic algorithm-II (NSGA-II). An experimental study on dynamic behaviour of a sandwich beam with 3D printed hexagonal honeycomb core filled with magnetorheological elastomer (MRE) was presented by Sharif et al. [12]. A comprehensive investigation about dynamic characterization of 3D printed lightweight structures was presented by Refat et al. [13]. Experimental and numerical analyses of the static properties of architectural cores and the dynamic behavior of 3D printed sandwich structures made with an auxetic or non-auxetic core were presented by Hamrouni et al. [14]. The influences of temperature and porosity on free vibration characteristics of a doubly-curved skew laminated sandwich composite structures with 3D printed PLA core was presented by Kallannavar and Kattimani [15]. The efficiency of Auxetic cores in sandwich beams subjected to low-velocity impact was presented by Hedayatian et al. [16]. Gan et al. [17] reported a comprehensive solution including analytical, numerical and experimental solutions for dynamic failure of 3D printed negative-stiffness meta-sandwich structures under repeated impact loadings. xperimental and numerical investigation of the structural behavior of a 3D printed bio-based anti-trichiral sandwich structure made of PLA was reported by Hamrouni et al. [18]. Experimental investigation and simulation of 3D printed sandwich structures with novel core topologies under bending loads were presented by Eryildiz [19]. Zhang et al. [20] developed a design method for bending and shear resistances of 3D printed beetle elytron inspired sandwich plate (beetle elytron plate) based on experimental, numerical and analytical methodologies. Jiang and Li [21] examined numerical and experimental investigation on 3D printed Auxetic mechanical metamaterial with chiral cells and re-entrant cores. Najafi, Ahmadi and Liaghat [22] evaluated the flexural behavior, energy absorption and the stiffness of fully integrated 3D printed polymeric sandwich beams, made of square node anti-tetra chiral, arrowhead and re-entrant auxetic cores, compared with the conventional honeycomb core. In another investigation, Najafi et al. [23] applied experimental and numerical assessment for investigation the influence of auxetic core topologies on the mechanical characteristics of fully integrated 3D printed polymeric sandwich structures. Due to the potential of these structures in practical application, Zhang et al. [24] investigated studied vibration tests of 3D printed satellite structure made of lattice sandwich panels. Broon et al. [25] performed linking material properties investigations, field Experiments, shaking table tests and FEM modeling for the possibility of using 3D Printed polymer models for modal tests on shaking tables. Chai et al. [26] investigated vibration characteristics of simply supported pyramidal lattice sandwich plates on elastic foundation theoretically and experimentally. Li et al. [27] used ABAQUS software and experimental tests for investigation the Large amplitude vibration of sandwich plates with 3D printed auxetic lattice core. They used 3D Re-entrant auxetic cell with gradient internal cell angles and cell wall aspect ratios. Wang et al. [28] performed an investigation about vibration and damping characteristics of 3D printed Kagome lattice with viscoelastic material filling by employing numerical and experimental approaches. Zamani et al. [29] presented a novel auxetic honeycomb core model for sandwich structures with increasing natural frequencies by employing 3D finite element procedure. Meng et al. [30] investigated an inverse approach to the accurate modelling of 3D-printed sandwich panels with lattice core using finite element method. The above literature review shows the influences of graded auxetic and non-auxetic cell including Re-entrant, the conventional hexagonal honeycomb and anti-tetrachiral on free and forced vibration of sandwich beam has not been investigated so far. In this investigation, four different FG patterns are assumed for each auxetic cell along the thickness of sandwich beam. The effective mechanical properties of various graded cells are estimated by analytical relations. Then, the higher order shear deformation theory was applied for prediction the displacements field. Finally, the FEM and Lagrange equations are employed for obtaining the effective stiffness and mass matrices of 3D printed

sandwich beam. Also, for solving the forced vibration of sandwich beam, Newmark integration method was applied in each time domain. The influences of various parameters such as different auxetic cells, various FG patterns of cells, various angles of auxetic cells, aspect ratio, boundary conditions on natural frequencies and forced vibration behavior of sandwich structure have been investigated.

2. Geometry and formulations

2.1. Description of geometry:

The sandwich beam is depicted in Figure 1 with length (a), total thickness (t) and with (b). Also, the various cells including two auxetic cells and conventional honey comb with different thickness patterns are shown in this figure.
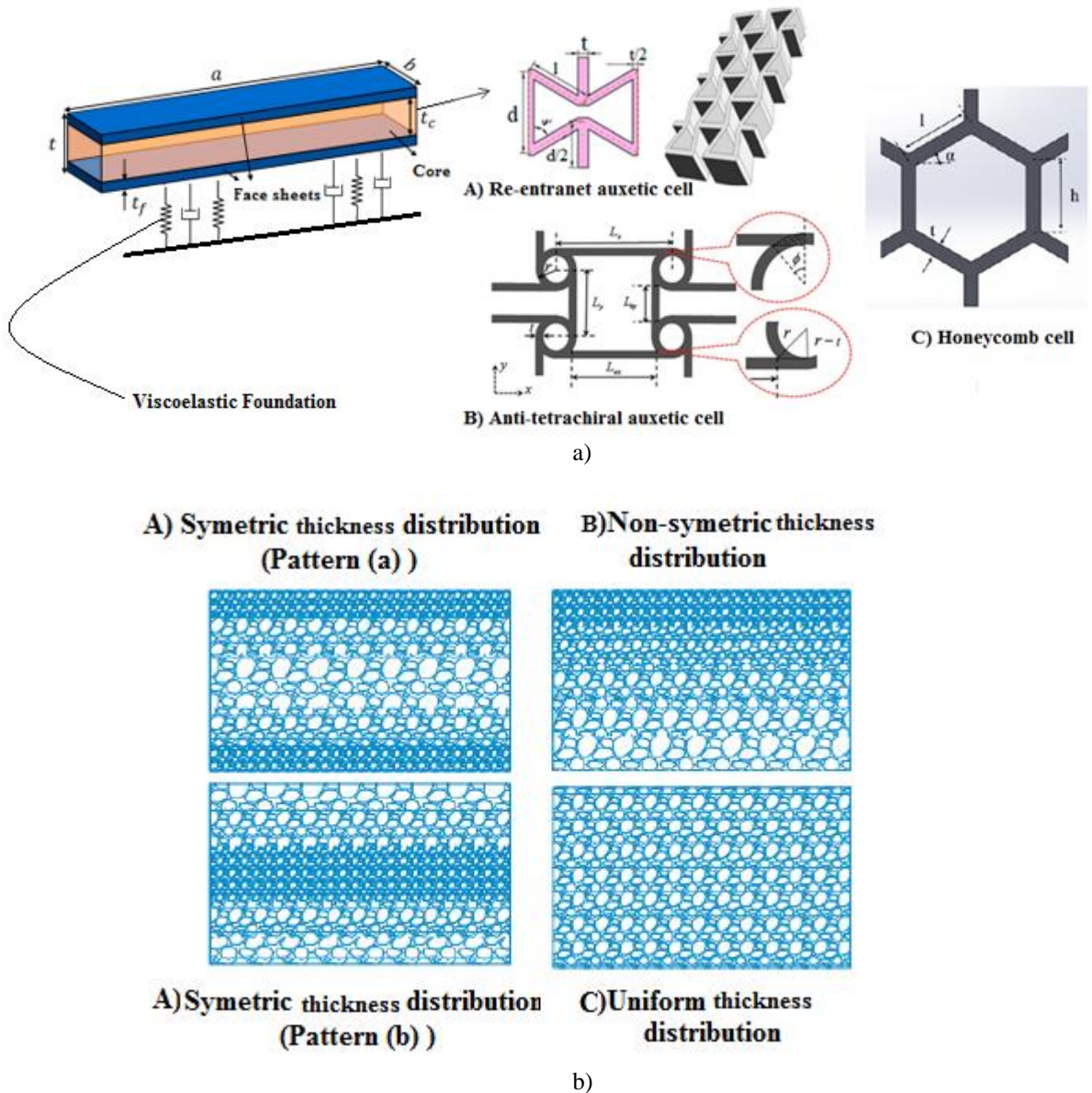

a)

b)

Figure 1: Figure 1: The schematic of 3D printed sandwich beam a) various cells of core b) different pattern of each cell along the thickness of structures

2.2. *Obtaining the effective mechanical properties of auxetic and non-auxetic cells*

For obtaining the effective mechanical properties of FG cells of sandwich beam, the effective mechanical properties of each cell including Young modulus, shear modulus, Poisson ratio and density of each cell should be obtained by analytical relations. For this regard, the mechanical properties of each cells (A, B, C) are given in relations (1-3):

a) Mechanical properties of Cell-A: (Re-entrant auxetic cell) [31]

$$E = E_C \left(\frac{t}{l}\right)^3 \frac{\cos \psi}{\left(\frac{d}{l} + \sin \psi\right) \sin^2 \psi}$$ (1)

$$G = G_C \left(\frac{t}{l}\right) \frac{\cos \psi}{\frac{d}{l} + \sin \psi}$$

$$\rho = \rho_C \frac{t/l \, (d/l + 2)}{2 \cos \psi \left(\frac{d}{l} + \sin \psi\right)}$$

$$\upsilon = \frac{-\sin \psi \left(1 - \left(\frac{t}{l}\right)^2\right)}{\left(tg^2 \psi + \left(\frac{t}{l}\right)^2\right)\left(\frac{d}{l} - \sin \psi\right)}$$

In the above equation, l, d, t, ψ and are the length of the inclined, vertical cell rib, the thickness of the cell and auxetic core interior angle, respectively. E,G, ρ are the Young modulus, shear modulus and mass density of Re-entrant auxetic cell. It is mentioned that E_c, G_c, ρ_c are the Young modulus, shear modulus and density of material which has been used for fabrication of Re-entrant auxetic cell. It is mentioned that ν, ν_c is the Poisson ratio of Re-entrant auxetic cell and the Poisson ratio of material which has been utilized for fabrication of the cell, respectively. These definitions (E,G, ρ , ν E_c, G_c, ρ_c, ν_c) are true for another cells.

b) Mechanical properties of Cell-B: (Anti-tetrachiral auxetic cell)

$$E = \frac{E_C \beta^3}{6(1 - 0.5\beta)^2} \left[\frac{1}{\alpha - 2\sqrt{2\beta - \beta^2}} \right], \quad \alpha = L/r \,, \ \beta = t/r$$ (2)

$$G = \frac{\alpha + \pi}{\alpha^2} \beta \, G_c$$

$$\rho = 2(t/l) + \left[1 + \frac{\pi}{rl}\right]$$

$$\nu = -1$$

In the above equation α and β are the dimensionless parameters. t is the thickness of cell. It is assumed $L_x = L_y = L$ and is shown in the Fig 1 a. It describes as the distance between the two centers of the circle.

c) Mechanical properties of Cell-C (Conventional honeycomb)

$$E = E_c (\frac{t}{l})^3 \frac{\cos\alpha}{(\frac{h}{l} + \sin\alpha)\sin^2\alpha}$$

$$G = G_c (\frac{t}{l})^3 \frac{(\frac{h}{l} + \sin\alpha)}{(\frac{h}{l})^2 (1 + 2\frac{h}{l})\cos\alpha}$$

$$\rho = \rho_c \frac{t/l\,(h/l+2)}{2\cos\alpha(\frac{d}{l} + \sin\alpha)}$$

$$\nu = \frac{\cos^2(\alpha)}{(\frac{h}{l} + \sin\alpha)\sin\alpha}$$

(3)

In the above equation, α is the interior angle of cell which is shown in figure 1. t is the thickness of structure. l, h are the length of the inclined and vertical cell.

2.3. Obtaining the effective mechanical properties of functionally graded cells

In this investigation, unlike previous researches, the thickness of cells can be followed as FG relation. On the other hand, the thickness of cells is varied along the thickness. By this way, the porosity volume of cells is changed along the thickness of Sandwich beam. Four FG patterns are considered for the thickness of cells along the thickness of structure. The relation of thickness cells along the thickness of sandwich beam follows as the following relations: [32-35]

For pattern A) a
$$t(z) = t(1 - e_0 \cos(\pi z / h))$$
For pattern A) b
$$t(z) = t(1 - e_0 (1 - \cos(\pi z / h)))$$
For pattern B)
$$t(z) = t(1 - e_0 \cos(\pi z / 2h + \pi / 4))$$
For Pattern C)
$$t(z) = t(1 - e_0)$$

(4)

In the above relation, e_0 is the thickness coefficient and its values is between zero and one. By replacing the Eq.4 into Eq.s (1-3), the effective mechanical properties of FG graded cells could be estimated.

2.4. Displacement field and strain

The displacement fields of core and face sheets are based on third order shear deformation theory. The same theory is considered for face sheets and core due to the structure is integrally printed (The delamination is not considered for these structures). This theory provides more flexibility than Euler Bernoulli and Timoshenko theories. Therefore, it is suitable for structures which are fabricated by polymer 3D printing.

$$u\left(x,z,t\right)=u_0\left(x,t\right)+z\,\Phi_x\left(x,t\right)-4\frac{z^3}{3h^2}\left[\Phi_x\left(x,t\right)+\frac{\partial w_0\left(x,t\right)}{\partial x}\right] \tag{5}$$

$$w\left(x,z,t\right)=w_0\left(x,t\right) \tag{6}$$

where u and w are the displacement components in the x and z directions respectively. u_0 and w_0 are the midplane displacements and Φ_x is the bending rotation of x-axis. t denotes time and h is the total thickness of the sandwich beam. The matrix form of the displacement field is as:

$$\bar{u}=\begin{bmatrix} u \\ w \end{bmatrix}=\begin{bmatrix} 1 & 0 & -4\dfrac{z^3}{3h^2} & \left(z-4\dfrac{z^3}{3h^2}\right) \\ 0 & 1 & 0 & 0 \end{bmatrix}\begin{bmatrix} u_0 \\ w_0 \\ \dfrac{\partial w_0}{\partial x} \\ \Phi_x \end{bmatrix}= \tag{7}$$

$$[Z_C][\bar{U}]$$

where

$$\left[\bar{U}\right]=\begin{bmatrix} u_0 \\ w_0 \\ \dfrac{\partial w_0}{\partial x} \\ \Phi_x \end{bmatrix}$$

$$\left[Z_c\right]=\begin{bmatrix} 1 & 0 & -4\dfrac{z^3}{3h^2} & \left(z-4\dfrac{z^3}{3h^2}\right) \\ 0 & 1 & 0 & 0 \end{bmatrix} \tag{8}$$

The strain–displacement relations can be described in a matrix form as:

$$[\varepsilon] = \begin{bmatrix} \varepsilon_{xx} \\ \gamma_{xz} \end{bmatrix} = \begin{bmatrix} 1 & \left(z - 4\dfrac{z^3}{3h^2}\right) & -4\dfrac{z^3}{3h^2} & 0 \\ 0 & 0 & 0 & \left(1 - 4\dfrac{z^2}{h^2}\right) \end{bmatrix} \begin{bmatrix} \dfrac{\partial u_0}{\partial x} \\ \dfrac{\partial \Phi_x}{\partial x} \\ \dfrac{\partial^2 w_0}{\partial x^2} \\ \Phi_x + \dfrac{\partial w_0}{\partial x} \end{bmatrix} = \tag{9}$$

$[z][\bar{\varepsilon}]$

where $[\bar{\varepsilon}]$ is expressed in the following equation:

$$[\bar{\varepsilon}] = \begin{bmatrix} \dfrac{\partial}{\partial x} & 0 & 0 & 0 \\ 0 & 0 & 0 & \dfrac{\partial}{\partial x} \\ 0 & \dfrac{\partial^2}{\partial x^2} & 0 & 0 \\ 0 & 0 & 1 & 1 \end{bmatrix} [\bar{U}] = [d][\bar{U}] \tag{10}$$

So, [ε] can be presented in the following matrix form:

$$[\varepsilon] = [Z][d][\bar{U}] \tag{11}$$

The stress- strain relationship for a 3D printed sandwich beam is as the following:

$$[\sigma] = [D][\varepsilon] \tag{12}$$

where [σ], [ε], [D] and its components are:

$$[\sigma] = \begin{bmatrix} \sigma_{xx} & \sigma_{xz} \end{bmatrix}^T \tag{13-1}$$

$$[\varepsilon] = \begin{bmatrix} \varepsilon_{xx} & \gamma_{xz} \end{bmatrix}^T \tag{13-2}$$

$$[D] = \begin{bmatrix} Q_{11}(z) & 0 \\ 0 & Q_{55}(z) \end{bmatrix} \tag{14}$$

For cores:

$$Q_{11}(z) = \frac{E(z)}{1 - v^2} \tag{15-1}$$

$$Q_{55}(z) = G(z) \tag{15-2}$$

For face sheets:

$$Q_{11} = E_C / (1 - v_C^2) \tag{16-1}$$

$$Q_{55} = G_C \tag{16-2}$$

In this research, the beam is supported by the viscoelastic foundation. The Kelvin-Voight linear model is used for modeling of the viscoelastic foundation. The relationship between force per unit area and deflection in this model can be calculated according to the following equation [36]:

$$P(x,t) = k_w w(x,t) + c_d \frac{\partial w(x,t)}{\partial t} \tag{17}$$

Where k_w is the elastic coefficient of the foundation in terms of (N/m^3), and C_d is the damping coefficient of the foundation in terms of $(N.s/m^3)$.

3. Finite element model of governing equations

The approximation of the displacement field in each element of the sandwich beam is as follows:

$$\left[\bar{U}^{(e)}(x,t) \right] = \left[N(x) \right] \left[Q^{(e)}(t) \right] \tag{18}$$

$\left[Q^{(e)}(t) \right]$ is nodal degrees of freedom of the beam element and $[N(x)]$ (its terms is given in the appendix) is shape function matrix and its components are shown in the appendix. $\left[Q^{(e)}(t) \right]$ contains u_i, w_i, $\frac{\partial w_i}{\partial x}$ and Φ_i. For u_i and Φ_i, the linear approximation is used and for approximation of w_i and $\frac{\partial w_i}{\partial x}$, the Hermitian element of the Euler-Bernoulli beam is used.

By replacing the equation 18 in 11:

$$\left[\bar{\varepsilon} \right] = \left[B \right] \left[Q^{(e)} \right] \tag{19}$$

In which [B]=[d] $[N(x)]$ (its terms is reported in appendix) represents the derivative of the matrix of the shape functions in terms of x and is explained in the appendix. The velocity components are obtained from the time derivative of the displacement field as follows:

$$\left[\dot{\bar{U}} \right] = \left[N(x) \right] \left[\dot{Q}^{(e)}(t) \right] \tag{20}$$

where $\left[\dot{Q}^{(e)}(t) \right]$ is the velocity component of element nodes.

The equation of motion of is extracted by using the Lagrange equations as follows:

$$\left\{ \frac{d}{dt} \left(\frac{\partial T}{\partial \dot{Q}} \right) \right\} + \left\{ \frac{\partial R}{\partial \dot{Q}} \right\} + \left\{ \frac{\partial U}{\partial Q} \right\} = F \tag{21}$$

In the above equation, kinetic energy is a function of the dissipation of the Rayleigh and the total potential energy and the total force on the beam.

The kinetic energy and the total potential energy are defined as follow:

$$T^{(e)} = T_{Core}{}^{(e)} + 2T_{Face\ sheets}{}^{(e)} =$$

$$\frac{1}{2} \iiint \left[\dot{\bar{U}} \right]^T [Z_c]^T \rho(z) [Z_c] \left[\dot{\bar{U}} \right] dx\ dy\ dz + \iiint \left[\dot{\bar{U}} \right]^T [Z_c]^T \rho_C [Z_c] \left[\dot{\bar{U}} \right] dx\ dy\ dz =$$

$$\frac{1}{2} b \int_0^{l^{(e)}} \left[\dot{\bar{U}} \right]^T (\int_{-t_c/2}^{t_c/2} [Z_c]^T \rho(z) [Z_c] dz) \left[\dot{\bar{U}} \right] dx + \int_0^{l^{(e)}} \left[\dot{\bar{U}} \right]^T (\int_{-t_c/2-t_f}^{t_c/2+t_f} [Z_c]^T \rho_C [Z_c] dz) \left[\dot{\bar{U}} \right] = \tag{22}$$

$$\frac{1}{2} b \int_0^{l^{(e)}} (\left[\dot{Q}^{(e)} \right]^T [N]^T [\bar{Z}]_{CORE} [N] \left[\dot{Q}^{(e)} \right] + \left[\dot{Q}^{(e)} \right]^T [N]^T [\bar{Z}]_{FACE\ SHEETS} [N] \left[\dot{Q}^{(e)} \right]) dx$$

Total potential energy of system is as:

$$\tag{23}$$

$$U^{(e)} = U_1^{(e)} + U_2^{(e)} = \frac{1}{2}\int \varepsilon^T \sigma \, dV + \frac{1}{2}\iint k_w w^2 \, dx \, dy$$

$$U_1^{(e)} = U_{Core}^{(e)} + 2U_{Face\ sheets}^{(e)}$$

$$= \frac{1}{2}b\int_0^{l^{(e)}} \int_{-t_c/2}^{t_c/2} \left[Q^{(e)}\right]^T [B]^T [Z]^T [D]_{Core} [Z][B]\left[Q^{(e)}\right] dx\, dz +$$

$$b\int_0^{l^{(e)}} \int_{-t_c/2-t_f}^{t_c/2+t_f} \left[Q^{(e)}\right]^T [B]^T [Z]^T [D]_{Face\ SHEETS} [Z][B]\left[Q^{(e)}\right] dx\, dz$$

$$+ \frac{1}{2}b\int_0^{l^{(e)}} \left[Q^{(e)}\right]^T \left[\bar{N}\right]^T k_w \left[\bar{N}\right]\left[Q^{(e)}\right] dx =$$

$$\frac{1}{2}\left[Q^{(e)}\right]^T \left(b\int_0^{l^{(e)}} [B]^T \left[\bar{D}\right]_{Core} [B]dx\right)\left[Q^{(e)}\right] +$$

$$\frac{1}{2}\left[Q^{(e)}\right]^T \left(b\int_0^{l^{(e)}} [B]^T \left[\bar{D}\right]_{FACE\ SHEETS} [B]dx\right)\left[Q^{(e)}\right] +$$

$$+ \frac{1}{2}\left[Q^{(e)}\right]^T \left(b\int_0^{l^{(e)}} \left[\bar{N}\right]^T k_w \left[\bar{N}\right] dx\right)\left[Q^{(e)}\right]$$

$[\bar{Z}]$ and $[\bar{D}]$ are defined as follow and $\bar{N}$ is presented in appendix:

$$\left[\bar{D}\right]_{CORE} = \int_{-\frac{t_C}{2}}^{\frac{t_C}{2}} [Z]^T [D][Z] \, dz$$

$$\left[\bar{D}\right]_{FACE\ SHEETS} = [D]\int_{-\frac{t_C}{2}-t_f}^{\frac{t_C}{2}+t_f} [Z]^T [Z] \, dz \tag{24}$$

$$\left[\bar{Z}\right]_{Core} = \int_{-t_c/2}^{t_c/2} [Z_c]^T \rho(z)[Z_c] \, dz$$

$$\left[\bar{Z}\right]_{FACE\ SHEETS} = 2\rho\int_{-t_c/2-t_f}^{t_c/2+t_f} [Z_c]^T [Z_c] \, dz$$

Since the damping of the viscoelastic foundation is a function of the Rayleigh dissipation (R). So, the equation of Rayleigh dissipation matrix for each element of the beam is:

$$R^{(e)} = \frac{1}{2}\iint c_d \dot{w}^2 \, dx\, dy = \frac{1}{2}b\int_0^{l^{(e)}} \left[\dot{Q}^{(e)}\right]^T \left[\bar{N}\right]^T c_d \left[\bar{N}\right]\left[\dot{Q}^{(e)}\right] dx =$$

$$\frac{1}{2}\left[\dot{Q}^{(e)}\right]^T \left(b\int_0^{l^{(e)}} \left[\bar{N}\right]^T c_d \left[\bar{N}\right] dx\right)\left[\dot{Q}^{(e)}\right] \tag{25}$$

If $p_z(t)$ is the external force of the beam, the work performed is defined by equation (26):

$$W_f^{(e)} = \frac{1}{2}\iint \begin{bmatrix} 0 \\ p_z \\ 0 \\ 0 \end{bmatrix} w \, dA = \left[Q^{(e)}\right]^T \left(b\int_0^{l^{(e)}} \left[\bar{N}\right]^T \begin{bmatrix} 0 \\ p_z \\ 0 \\ 0 \end{bmatrix} dx\right) \tag{26}$$

Therefore, the mass matrix $\left[M^{(e)} \right]$, The stiffness matrix caused by strain $\left[K_{\varepsilon}^{(e)} \right]$, the stiffness matrix due to the elastic properties of the foundation $\left[K_{kw}^{(e)} \right]$, the damping matrix due to damping property of foundation $\left[C^{(e)} \right]$ and the external force matrix for each element of the beam $\left\{ F^{(e)} \right\}$ are as following:

$$\left[M^{(e)} \right] = b \int_0^{l^{(e)}} \left[N \right]^T \left[\bar{Z} \right]_{Core} \left[N \right] dx + 2b \int_0^{l^{(e)}} \left[N \right]^T \left[\bar{Z} \right]_{FACE\ SHEETS} \left[N \right] dx \tag{27}$$

$$\left[K_{\varepsilon}^{(e)} \right] = b \int_0^{l^{(e)}} \left[B \right]^T \left[\bar{D} \right]_{CORE} \left[B \right] dx + 2b \int_0^{l^{(e)}} \left[B \right]^T \left[\bar{D} \right]_{FACE\ SHEETS} \left[B \right] dx \tag{28}$$

$$\left[K_{kw}^{(e)} \right] = b \int_0^{l^{(e)}} \left[\bar{N} \right]^T k_w \left[\bar{N} \right] dx \tag{29}$$

$$\left[C^{(e)} \right] = b \int_0^{l^{(e)}} \left[\bar{N} \right]^T c_d \left[\bar{N} \right] dx \tag{30}$$

$$\left\{ F^{(e)} \right\} = b \int_0^{l^{(e)}} \left[\bar{N} \right]^T \begin{bmatrix} 0 \\ p_z \\ 0 \\ 0 \end{bmatrix} dx \tag{31}$$

After assembly of element matrices, the matrix form of the Lagrange equations is as:

$$\left[M \right] \left[\ddot{Q} \right] + \left[C \right] \left[\dot{Q} \right] + \left[K \right] \left[Q \right] = \left\{ F \right\} \tag{32}$$

Finally, Newmark method [38] is used to solve the governing equation (32) in time domain. In this method, the displacement and velocity vectors at time $t + \Delta t$ are approximated in terms of their values at time t according to the following equations:

$$\{\dot{Q}\}_{t+\Delta t} = \{\dot{Q}\}_t + \left[(1-\gamma)\left\{\ddot{Q}\right\}_t + \gamma \left\{\ddot{Q}\right\}_{t+\Delta t} \right] \Delta t \tag{33}$$

$$\{Q\}_{t+\Delta t} = \{Q\}_t + \{\dot{Q}\}_t \, \Delta t + \left[\left(\frac{1}{2} - \beta \right)\left\{\ddot{Q}\right\}_t + \beta \left\{\ddot{Q}\right\}_{t+\Delta t} \right] \Delta t^2 \tag{34}$$

By choosing the parameters $\beta = 1/4$ and $\gamma = 1/2$, the solution method is called the mean acceleration method and is unconditionally stable in linear analysis. Now the equilibrium Eq. (35) for time is rewritten as follows:

$$\left[M \right] \left\{ \ddot{Q} \right\}_{t+\Delta t} + \left[C \right] \left\{ \dot{Q} \right\}_{t+\Delta t} + \left[K \right] \left\{ Q \right\}_{t+\Delta t} = \left\{ F \right\}_{t+\Delta t} \tag{35}$$

From the solution of Eq. $\left\{Q^{\bullet\bullet}\right\}_{t+\Delta t}$ (34) is obtained and $\left\{Q^{\bullet}\right\}_{t+\Delta t}$ is obtained by replacing $\left\{Q^{\bullet\bullet}\right\}_{t+\Delta t}$ in Eq. (33).

Now $\left\{Q^{\bullet\bullet}\right\}_{t+\Delta t}$ and $\left\{Q^{\bullet}\right\}_{t+\Delta t}$ are obtained in terms of $\left\{Q\right\}_{t+\Delta t}$, and by replacing these expressions in Eq. (38), the following relation is obtained:

$$\left[\hat{K}\right]\left\{Q\right\}_{t+\Delta t} = \left\{\hat{F}\right\} \tag{36}$$

Ithe above equation, the matrices $\left[\hat{K}\right]$ and $\left\{\hat{F}\right\}$ are defined as follows:

$$\left[\hat{K}\right] = \frac{1}{\beta\Delta t^2}\left[M\right] + \left[K\right] + \frac{\gamma}{\beta\Delta t}\left[C\right] \tag{37}$$

$$\left\{\hat{F}\right\} = \left\{F\right\}_{t+\Delta t} + \left[M\right]\left(\frac{1}{\beta\Delta t^2}\left\{Q\right\}_t + \frac{1}{\beta\Delta t}\left\{\dot{Q}\right\}_t + \left(\frac{1}{2\beta}-1\right)\left\{\ddot{Q}\right\}_t\right) +$$
$$\left[C\right]\left(\frac{\gamma}{\beta\Delta t}\left\{Q\right\}_t + \left(\frac{\gamma}{\beta}-1\right)\left\{\dot{Q}\right\}_t + \frac{\Delta t}{2}\left(\frac{\gamma}{\beta}-2\right)\left\{\ddot{Q}\right\}_t\right) \tag{38}$$

with the known initial conditions and marching through time, the Eq. (38) is solved and displacements at each time are obtained.

It is mentioned that the boundary condition in this investigation is considered, are as the following:

$$u_0 = w_0 = \frac{\partial w_0}{\partial x} = \Phi_x = 0 \qquad @ \ x=0, L_{(e)} \qquad \text{Clamped-Clamped} \tag{39}$$

$$u_0 = \frac{\partial w_0}{\partial x} = \Phi_x = 0 \qquad @ \ x=0, L_{(e)} \qquad \text{Simple-Simple} \tag{40}$$

4. Results and discussion

4.1. Validation

To sure, the accuracy of results, a validation was performed. Due to it is not possible to enter the mechanical properties of FGM to the ANSYS-WORKBENCH and model FG cores, it is sufficient to consider simplified state of the problem, for this target, the mechanical properties of core should be assumed same as face sheets in MATLAB code and compare the results with results of ANSYS-WORK BENCH. The comparison between results of MATLAB code and ANSYS-WORK BENCH is given in table 1. As can be seen, an excellent agreement is governed between them. The Clamped-Clamped boundary condition is assumed for verification section. The difference between present MATLAB CODE results and ANSYS WORKBENCH is related to their the ANSYS WORK BENCH use Euler Bernoulli theory while in MATLAB CODE, higher order shear deformation theory is employed for simulation of beam [37, 38].

Geometry: L=70cm, b=10cm, h=10cm

Mechanical properties :E=3600MPa , $\rho = 1.25g\ /cm^3$, $\nu = 0.39$

Table 1: The comparison between the present result (Hz) and ANSYSY WORKBENCH (Isotropic homogeneous C-C beam)

Results	ω_1	ω_2	ω_3	ω_4	ω_5	ω_6
MATLABCODE	321.05	321.05	672.41	777.39	777.39	1230.7
ANSYS-WORKBENCH	328.12	328.12	684.94	783.223	778.223	1245.12
Error percentage	0.31%	0.31%	1.78%	1.78%	1.78%	1.21%

4.2. Numerical results

The first six natural frequencies of various cells with different thickness distribution along the thickness of sandwich beam is depicted in table 2 to 4. The geometries of cells and interior angle are assumed as the following:

For Re-entrant auxetic cell: $\psi = 60^0$, $l/d = 1$, l=1cm, for anti-tetrachiral auxetic cell L/r=5 ,r=0.14 cm,   For conventional honeycomb :h/l=1 , $\alpha = 30^0$. It is mentioned that the total length of structure is constant (L=70cm) and H is the thickness of core. Besides, the thickness of face sheets (h_f) is 0.2 H.

It is mentioned that the face sheets and core made of PLA. The mechanical properties of PLA are as the following.

E=3600MPa , $\rho = 1.25g/cm^3$, $\nu = 0.39$

Natural frequencies have been normalized by the following relation:

$$\Omega = \omega L \sqrt{\frac{\rho_{PLA}}{E_{PLA}}(1-\upsilon^2)} \tag{41}$$

The influences of Re-entrant auxetic cell with various thickness pattern of cells along the thickness of sandwich beam, thickness coefficient and aspect ratio on natural frequencies of 3D printed sandwich beam are shown in table 2. It is obvious by increasing the thickness coefficient, the natural frequencies of structure decrease and the reason belong to increasing the thickness ratio causes the volume of pores in the structure to increase. This phenomenon leads the stiffness of structure considerably decrease. It is mentioned that by increasing the aspect ratio (L/H)in any pattern of Re-entrant auxetic cell, the natural frequencies are decreased. Its reason is related to increasing the length of beam (keep the thickness constant), the stiffness of structure significantly decreases. It is mentioned that in Re-entrant auxetic cell, TD1 has more natural frequencies than others thickness distributions. These phenomena are governed for another cells including anti-tetrachiral auxetic cell and conventional honeycomb cell. Also, for Re-entrant auxetic cell, TD3 has the minimum values of natural frequencies than others thickness distributions. This content is governed for another cells. The amounts of natural frequencies for anti-tetrachiral auxetic cell with various thickness patterns along the thickness is given in table 3. It is mentioned that by increasing the thickness coefficient and aspect ratio, the amount of natural frequencies decreases due to the reduction of the structure stiffness. It is mentioned that anti-tetrachiral auxetic cell with TD1 has the most natural frequencies among various cells in conjunction with different thickness distribution (TD). The amounts of natural frequencies of anti-tetrachiral auxetic cell with another thickness distribution are generally lower than Re-entrant auxetic cell with same TD. On the other hand, the FG arrangements of cells along the thickness play a prominent role in free vibration behavior of 3D printed sandwich beam. For instance, in uniform thickness distribution, the amounts of natural frequencies of Re-entrant auxetic cell are more than anti-tetrachiral auxetic cell while by creating FG anti-tetrachiral auxetic cell along the thickness as TD1, the amounts of natural frequencies of anti-tetrachiral auxetic cell will be more than Re-entrant auxetic cell. It is not true that we say the Re-entrant auxetic cell generally have more natural frequencies than anti-tetrachiral auxetic cell. The amounts of natural frequencies of conventional honeycomb are given in table 4. This cell in any TD has the minimum amounts of natural frequencies than other cell in conjunction with same TD. By comparison between table 2 to 4, we understand that auxetic cores provide more rigidity than non-auxetic cells. The influence of interior angle and geometry of Re-entrant auxetic cell is given in table 5 and 6, respectively. By increasing the d/l (PD1, L/H=5, e₀=0.1, interior angle=60⁰), and interior angle (PD1, L/H=5, e₀=0.1, d/l=1), the natural frequencies increase. This phenomenon is governed for conventional honeycomb but in this cell by increasing the interior angle, the amounts of natural frequencies decrease. The influences of interior angle and geometry of this cell on free vibration of sandwich beam are given in table 7 and 8, respectively. The influences of (L/r) for anti-tetrachiral auxetic cell on natural frequencies of structure is reported in table 9. By increasing the (L/r), the amounts of natural frequencies decrease due to the reduction of structure stiffness.

Table 2: The influences of various thickness patterns, thickness coefficient and aspect ratio on natural frequencies of 3D printed sandwich beam with Re-entrant auxetic cell Re-entrant auxetic cell

TD1	L/H		ω_1	ω_2	ω_3	ω_4	ω_5	ω_6
	5	e_0=0.1	1.253801	1.611883	1.935245	2.287541	2.478364	2.618261
		e_0=0.3	1.197379	1.536367	1.841923	2.173849	2.350915	2.479492
		e_0=0.5	1.142211	1.462547	1.751743	2.067707	2.237409	2.353815
		e_0=0.7	1.102090	1.411130	1.687494	1.981009	2.138772	2.243848
	7	e_0=0.1	0.789894	1.004151	1.192083	1.393112	1.491937	1.557865
		e_0=0.3	0.754349	0.957157	1.134625	1.323874	1.415251	1.475298
		e_0=0.5	0.719593	0.911167	1.079074	1.259234	1.346921	1.400521
		e_0=0.7	0.694317	0.879135	1.039497	1.206435	1.287541	1.335095
	10	e_0=0.1	0.539134	0.685015	0.812784	0.949329	1.016103	1.060395
		e_0=0.3	0.514873	0.652956	0.773608	0.902147	0.963875	1.004194
		e_0=0.5	0.491151	0.621583	0.735732	0.858099	0.917338	0.953295
		e_0=0.7	0.473899	0.599731	0.708748	0.822119	0.876897	0.908759
TD2								
	5	e_0=0.1	1.153496	1.473185	1.757162	2.063361	2.220557	2.330251
		e_0=0.3	1.101589	1.404244	1.672466	1.960812	2.106421	2.206748
		e_0=0.5	1.050835	1.336768	1.590583	1.865072	2.004719	2.094896
		e_0=0.7	1.013923	1.289774	1.532245	1.786871	1.916341	1.997025
	7	e_0=0.1	0.726702	0.917794	1.082412	1.256587	1.336775	1.386501
		e_0=0.3	0.694001	0.874842	1.030239	1.194135	1.268065	1.313015
		e_0=0.5	0.662026	0.832807	0.979799	1.135829	1.206841	1.246463
		e_0=0.7	0.638771	0.803529	0.943863	1.088204	1.153637	1.188231
	10	e_0=0.1	0.496003	0.626104	0.738008	0.856295	0.910428	0.943752
		e_0=0.3	0.473683	0.596802	0.702436	0.813737	0.863632	0.893733
		e_0=0.5	0.451859	0.568127	0.668045	0.774005	0.821935	0.848433
		e_0=0.7	0.435987	0.548154	0.643543	0.741551	0.785731	0.808795
TD3								
	5	e_0=0.1	1.065731	1.360359	1.621698	1.903233	2.047076	2.146973
		e_0=0.3	1.017772	1.296694	1.543532	1.808643	1.941856	2.033184
		e_0=0.5	0.970883	1.234394	1.467961	1.720333	1.848105	1.930129
		e_0=0.7	0.936777	1.190994	1.414120	1.648210	1.766626	1.839956
	7	e_0=0.1	0.671418	0.847504	0.998966	1.159069	1.232341	1.277449
		e_0=0.3	0.641196	0.807841	0.950816	1.101463	1.168997	1.209744
		e_0=0.5	0.611654	0.769025	0.904264	1.047683	1.112556	1.148427
		e_0=0.7	0.590169	0.741991	0.871098	1.003754	1.063509	1.094774
	10	e_0=0.1	0.458264	0.578153	0.681113	0.789842	0.839301	0.869524
		e_0=0.3	0.437642	0.551095	0.648283	0.750587	0.796161	0.823439
		e_0=0.5	0.417478	0.524616	0.616543	0.713938	0.757721	0.781702
		e_0=0.7	0.402814	0.506173	0.593931	0.684003	0.724317	0.745182
TD4								
	5	e_0=0.1	1.028116	1.313617	1.567512	1.841471	1.982641	2.081517
		e_0=0.3	0.981851	1.252144	1.491958	1.749949	1.880732	1.971196
		e_0=0.5	0.936614	1.191976	1.418912	1.664504	1.789927	1.871284
		e_0=0.7	0.903714	1.150072	1.366871	1.594713	1.711018	1.783862
	7	e_0=0.1	0.647713	0.818383	0.965587	1.121455	1.193549	1.238502

	$e_0=0.3$	0.618566	0.780083	0.919046	1.065719	1.132201	1.172862
	$e_0=0.5$	0.590067	0.742601	0.874051	1.013683	1.077536	1.113414
	$e_0=0.7$	0.569348	0.716495	0.841992	0.971189	1.030033	1.061397
10	$e_0=0.1$	0.442094	0.558287	0.658355	0.764214	0.812882	0.843014
	$e_0=0.3$	0.422196	0.532159	0.626622	0.726229	0.771841	0.798335
	$e_0=0.5$	0.402744	0.506593	0.595943	0.690769	0.733837	0.757870
	$e_0=0.7$	0.388597	0.488787	0.574086	0.661806	0.701518	0.722463

1.1. Transient vibration under an impulsive load

In this section, the transient vibration analysis of sandwich beam fabricated by 3D printer is investigated. It is assumed that the beam is subjected to an impulsive pressure. According to (42), the maximum magnitude of impulsive pressure at t=0.005 s is equal to 0.2 MPa. The mechanical properties and geometry are same as 4.2. section. (free vibration analysis of sandwich beam)

$$P_z = \begin{cases} 40t \left(\dfrac{MPa}{s} \right) & t \leq 0.005 \\ 0 & t \geq 0.005 \end{cases} \tag{42}$$

For forced vibration analysis, the numerical results are obtained for middle point of the sandwich beam. Fig 2 and 3 show the time history of midpoint transverse displacement of the simply supported sandwich beam (S-S) for various thickness coefficients and aspect ratio L/h. By increasing the thickness ratio, the amplitude vibration increase due to the stiffness of structure decrease. Also, by increasing the aspect ratio, the amplitude vibration increase due to increasing the length of structure causes the reduction in the stiffness of 3D printed sandwich beam. The influence of aspect ratio ($e_0=0.5$, $\psi = 60^0$,l/d=1) on amplitude vibration is more than thickness coefficient. Time history of midpoint transverse displacement of the simply supported sandwich beam (S-S) for various thickness pattern (L/h=5, $\psi = 60^0$,l/d=1) is shown in Figure 4. The most amplitude vibration of 3D printed sandwich beam belong to TD1, TD2, TD3, TD4, respectively. The results of Fig 2 to Fig 4 are related to Re-entrant auxetic cell ($e_{0=0.5}$). The influences of various auxetic cell on free vibration of 3D printed sandwich beam is depicted in Fig 5. (TD2, e0=0.5, L/h=5, d/l= 1, h/l=1, L/r=3). The minimum amplitude of vibration is related to Re-entrant auxetic cell, Anti-tetrachiral and conventional honeycomb, respectively. Fig 6 shows the effect of elastic coefficient of foundation on time history of midpoint transverse displacement of the simply supported sandwich beam. In these results, damping coefficient of the foundation is considered to be zero $(C_d = 0)$. Results illustrate that by increasing the elastic coefficient of the foundation, the stiffness of sandwich beam increases and consequently, amplitude of transverse displacement decrease significantly. Figs 7 shows the effect of damping coefficient of foundation on time history of midpoint transverse displacement of the simply supported beam. In these results, elastic coefficient of the foundation is considered to be zero ($K_w = 0$). As it can be seen from these figures, by increasing damping of the foundation, amplitude of vibration decreases and vibration of beam can be seen in three situations such as under-damped, critically-damped and over-damped.

5. Conclusion

In current research, free and forced vibration of FG Sandwich beam surrounded by viscoelastic foundation fabricated by 3D printer based on higher order shear deformation theory is investigated. Three various cells in conjunction with four different thickness patterns of cells are considered along the thickness of structure. The effective mechanical properties of cells with various thickness distribution are estimated by analytical relations. Kelvin-voit model is employed for modeling viscoelastic foundation. Finally, the FEM and Lagrange equations are utilized for obtaining the equal stiffness and mass matrices of structure. The important achievement of this research are as the following:

Table 3: The influences of various thickness patterns, thickness coefficient and aspect ratio on natural frequencies of 3D printed sandwich beam with anti-tetrachiral auxetic cell Anti -tetrachiral auxetic cell

TD1	L/H		ω_1	ω_2	ω_3	ω_4	ω_5	ω_6
	5	e_0=0.1	1.365730	1.770032	2.000211	2.394423	2.655510	2.825521
		e_0=0.3	1.277772	1.755591	1.965635	2.347772	2.598278	2.780758
		e_0=0.5	1.207088	1.543165	1.889824	2.197551	2.401798	2.600743
		e_0=0.7	1.176777	1.479461	1.834371	2.083858	2.317957	2.487271
	7	e_0=0.1	0.956011	1.239021	1.400147	1.676094	1.858857	1.977865
		e_0=0.3	0.894434	1.228914	1.375945	1.643446	1.818795	1.946536
		e_0=0.5	0.844962	1.080216	1.322877	1.538286	1.681259	1.820520
		e_0=0.7	0.823744	1.035623	1.284059	1.458701	1.622574	1.741091
	10	e_0=0.1	0.546292	0.708012	0.800084	0.957768	1.062204	1.130208
		e_0=0.3	0.519109	0.702237	0.786254	0.939109	1.039311	1.112303
		e_0=0.5	0.482835	0.617266	0.755931	0.879020	0.960719	1.040297
		e_0=0.7	0.470911	0.591784	0.733748	0.833543	0.927183	0.994908
TD2								
	5	e_0=0.1	0.980472	1.252207	1.493588	1.753857	1.887473	1.980713
		e_0=0.3	0.936351	1.193604	1.421596	1.666694	1.790457	1.875736
		e_0=0.5	0.893213	1.136253	1.351996	1.585311	1.704011	1.780662
		e_0=0.7	0.861835	1.096308	1.302408	1.518843	1.628890	1.697471
	7	e_0=0.1	0.617697	0.780125	0.920050	1.068099	1.136259	1.178525
		e_0=0.3	0.589901	0.743616	0.875703	1.015015	1.077855	1.116063
		e_0=0.5	0.562722	0.707886	0.832829	0.965455	1.025815	1.059494
		e_0=0.7	0.542955	0.683000	0.802284	0.924973	0.980591	1.009996
	10	e_0=0.1	0.421603	0.532188	0.627307	0.727851	0.773864	0.802189
		e_0=0.3	0.402631	0.507282	0.597071	0.691676	0.734087	0.759673
		e_0=0.5	0.384086	0.482908	0.567838	0.657904	0.698645	0.721168
		e_0=0.7	0.370589	0.465931	0.547012	0.630318	0.667845	0.687476
TD3								
	5	e_0=0.1	0.905871	1.156305	1.378443	1.617748	1.740015	1.824927
		e_0=0.3	0.865106	1.102194	1.312002	1.537347	1.650578	1.728206
		e_0=0.5	0.825248	1.049232	1.247767	1.462283	1.570885	1.640610
		e_0=0.7	0.796261	1.012345	1.202002	1.400972	1.501632	1.563963
	7	e_0=0.1	0.570699	0.720378	0.849121	0.985209	1.047489	1.085832
		e_0=0.3	0.545017	0.686665	0.808194	0.936244	0.993647	1.028282
		e_0=0.5	0.519906	0.653671	0.768624	0.890531	0.945673	0.976163
		e_0=0.7	0.501644	0.630692	0.740433	0.853191	0.903983	0.930558
	10	e_0=0.1	0.389524	0.491432	0.578946	0.671366	0.713406	0.739095
		e_0=0.3	0.371996	0.468431	0.551041	0.637999	0.676737	0.699923
		e_0=0.5	0.354856	0.445924	0.524062	0.606847	0.644063	0.664447
		e_0=0.7	0.342392	0.430247	0.504841	0.581403	0.615669	0.633405
TD4								
	5	e_0=0.1	0.873899	1.116574	1.332385	1.56525	1.685244	1.769289
		e_0=0.3	0.834573	1.064319	1.268164	1.487457	1.598622	1.675517
		e_0=0.5	0.796122	1.013181	1.206075	1.414828	1.521438	1.590591
		e_0=0.7	0.768157	0.977561	1.16184	1.355506	1.454365	1.516281
	7	e_0=0.1	0.550556	0.695626	0.820749	0.953237	1.014517	1.052727
		e_0=0.3	0.525781	0.663071	0.781189	0.905861	0.962371	0.996933
		e_0=0.5	0.501557	0.631211	0.742943	0.861631	0.915906	0.946402
		e_0=0.7	0.483939	0.609021	0.715693	0.825503	0.875528	0.902187
	10	e_0=0.1	0.375777	0.474544	0.559602	0.649579	0.690951	0.716562
		e_0=0.3	0.358867	0.452335	0.532629	0.617295	0.655435	0.678585
		e_0=0.5	0.342332	0.430602	0.506552	0.587154	0.623794	0.644192
		e_0=0.7	0.330307	0.415463	0.487973	0.562535	0.596292	0.614094

Table 4: The influences of various thickness patterns, thickness coefficient and aspect ratio on natural frequencies of 3D printed sandwich beam with Conventional honeycomb cell

Conventional honeycomb cell

TD1	L/H		ω_1	ω_2	ω_3	ω_4	ω_5	ω_6
	5	e_0=0.1	0.727204	0.934844	1.122416	1.326773	1.437414	1.518591
		e_0=0.3	0.694481	0.891093	1.068316	1.260833	1.363531	1.438105
		e_0=0.5	0.662483	0.848277	1.016011	1.199270	1.297697	1.365213
		e_0=0.7	0.639212	0.818456	0.978747	1.148986	1.240488	1.301432
	7	e_0=0.1	0.458139	0.582408	0.691408	0.808005	0.865323	0.903562
		e_0=0.3	0.437522	0.555151	0.658083	0.767847	0.820846	0.855673
		e_0=0.5	0.417364	0.528477	0.625863	0.730356	0.781214	0.812302
		e_0=0.7	0.402704	0.509898	0.602908	0.699732	0.746774	0.774352
	10	e_0=0.1	0.312698	0.397309	0.471415	0.550611	0.589343	0.615029
		e_0=0.3	0.298626	0.378714	0.448693	0.523245	0.559048	0.582433
		e_0=0.5	0.284868	0.360518	0.426725	0.497697	0.532056	0.552911
		e_0=0.7	0.274861	0.347844	0.411074	0.476829	0.508614	0.527083
TD2								
	5	e_0=0.1	0.669028	0.854447	1.019154	1.196749	1.287923	1.351546
		e_0=0.3	0.638922	0.814459	0.970031	1.137271	1.221724	1.279914
		e_0=0.5	0.609484	0.775325	0.922538	1.081742	1.162737	1.215042
		e_0=0.7	0.588075	0.748069	0.888702	1.036385	1.111478	1.158275
	7	e_0=0.1	0.421487	0.532321	0.627799	0.728826	0.775331	0.804173
		e_0=0.3	0.402521	0.507408	0.597539	0.692598	0.735478	0.761549
		e_0=0.5	0.383975	0.483028	0.568283	0.658781	0.699968	0.722949
		e_0=0.7	0.370487	0.466047	0.547441	0.631158	0.669109	0.689173
	10	e_0=0.1	0.287682	0.363141	0.428045	0.496651	0.528048	0.547376
		e_0=0.3	0.274736	0.346145	0.407413	0.471967	0.500907	0.518365
		e_0=0.5	0.262078	0.329514	0.387466	0.448923	0.476722	0.492091
		e_0=0.7	0.252872	0.317929	0.373255	0.430143	0.455706	0.469101
TD3								
	5	e_0=0.1	0.618123	0.789008	0.940585	1.103875	1.187304	1.245244
		e_0=0.3	0.590308	0.752083	0.895249	1.049013	1.126276	1.179247
		e_0=0.5	0.563131	0.715946	0.851417	0.997793	1.071898	1.119475
		e_0=0.7	0.543331	0.690777	0.820195	0.955956	1.024643	1.067174
	7	e_0=0.1	0.389418	0.491552	0.579400	0.672260	0.714757	0.740921
		e_0=0.3	0.371894	0.468548	0.551473	0.638849	0.678018	0.701652
		e_0=0.5	0.354759	0.446035	0.524473	0.607656	0.645282	0.666088
		e_0=0.7	0.342298	0.430354	0.505237	0.582177	0.616835	0.634969
	10	e_0=0.1	0.265793	0.335329	0.395046	0.458108	0.486795	0.504324
		e_0=0.3	0.253832	0.319635	0.376004	0.435344	0.461773	0.477595
		e_0=0.5	0.242137	0.304277	0.357595	0.414084	0.439478	0.453387
		e_0=0.7	0.233632	0.293548	0.344481	0.396722	0.420104	0.432206
TD4								
	5	e_0=0.1	0.596307	0.761898	0.909157	1.068053	1.149931	1.207280
		e_0=0.3	0.569474	0.726241	0.865336	1.014975	1.090825	1.143294
		e_0=0.5	0.543236	0.691346	0.822969	0.965412	1.038158	1.085345
		e_0=0.7	0.524154	0.667042	0.792785	0.924934	0.992391	1.034639
	7	e_0=0.1	0.375674	0.474662	0.560041	0.650444	0.692258	0.718331
		e_0=0.3	0.358768	0.452448	0.533047	0.618117	0.656677	0.680263
		e_0=0.5	0.342239	0.430709	0.506949	0.587936	0.624971	0.645783

	e_0=0.7	0.330217	0.415567	0.488355	0.563284	0.597419	0.615610
10	e_0=0.1	0.256412	0.323806	0.381846	0.443242	0.471472	0.488948
	e_0=0.3	0.244874	0.308652	0.363441	0.421213	0.447238	0.463034
	e_0=0.5	0.233592	0.293822	0.345647	0.400646	0.425645	0.439565
	e_0=0.7	0.225386	0.283492	0.332970	0.383847	0.406881	0.419029

Table 5: The influences of various interior angle on natural frequencies of 3D printed sandwich beam (Re-entrant auxetic cell, TD1, L/H=5, e_0=0.1, d/l=1)

Interior angle(ψ)	ω_1	ω_2	ω_3	ω_4	ω_5	ω_6
30^0	1.068541	1.268743	1.647239	1.832964	2.114952	2.185294
45^0	1.118645	1.328745	1.709632	1.092648	2.179843	2.278812
60^0	1.142211	1.462547	1.751743	2.067707	2.237409	2.353815

Table 6: The influences of various (d/l) on natural frequencies of 3D printed sandwich beam (Re-entrant auxetic cell, TD1, L/H=5, e_0=0.1, l/d=1, $\psi = 60^0$)

(d/l)	ω_1	ω_2	ω_3	ω_4	ω_5	ω_6
3	1.243869	1.594908	1.912903	2.261038	2.449963	2.582136
2	1.210745	1.553957	1.865606	2.207278	2.394028	2.525644
1	1.142211	1.462547	1.751743	2.067707	2.237409	2.353815

Table 7: The influences of various interior angle on natural frequencies of 3D printed sandwich beam (conventional honeycomb cell, TD1, L/H=5, e_0=0.1, h/l=1)

Interior angle(α)	ω_1	ω_2	ω_3	ω_4	ω_5	ω_6
30^0	0.662483	0.848277	1.016011	1.199271	1.297697	1.365213
45^0	0.658746	0.791623	0.989341	1.000230	1.139637	1.204825
60^0	0.650738	0.752842	0.978237	0.983281	1.089424	1.110344

Table 8: The influences of various h/l on natural frequencies of 3D printed sandwich beam (conventional honeycomb cell, TD1, L/H=5, e_0=0.1, l/d=1, $\alpha = 30^0$)

h/l	ω_1	ω_2	ω_3	ω_4	ω_5	ω_6
3	0.728432	0.993022	1.389432	1.459431	1.783291	1.890312
2	0.684921	0.909342	1.124345	1.385933	1.432952	1.500893
1	0.662483	0.848277	1.016011	1.199274	1.297697	1.365213

Table 9: The influences of various L/r on natural frequencies of 3D printed sandwich beam (conventional honeycomb cell, TD1, L/H=5, e₀=0.1, h/l=1)

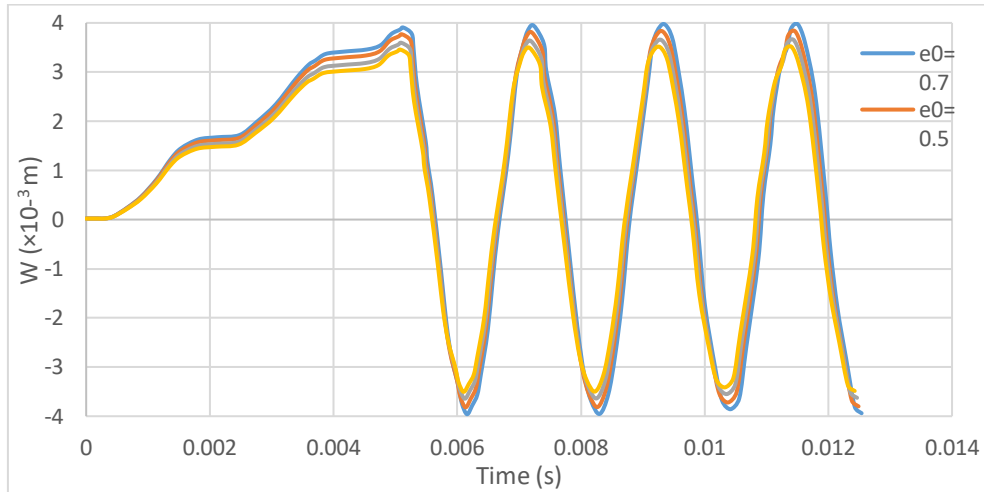| L/r	ω_1	ω_2	ω_3	ω_4	ω_5	ω_6
5	0.809371	0.901394	1.139351	1.378462	1.893821	2.013842
4	1.000341	1.120454	1.405301	1.778322	2.013583	2.220483
3	1.207088	1.543165	1.889824	2.197551	2.401798	2.600743

Fig 2. The influences of different thickness coefficient on time history of midpoint transverse displacement of the simply supported 3D printed sandwich beam (TD1,Re-entrant auxetic cell, l/d=1, $\psi = 60^0$,L/h=5)
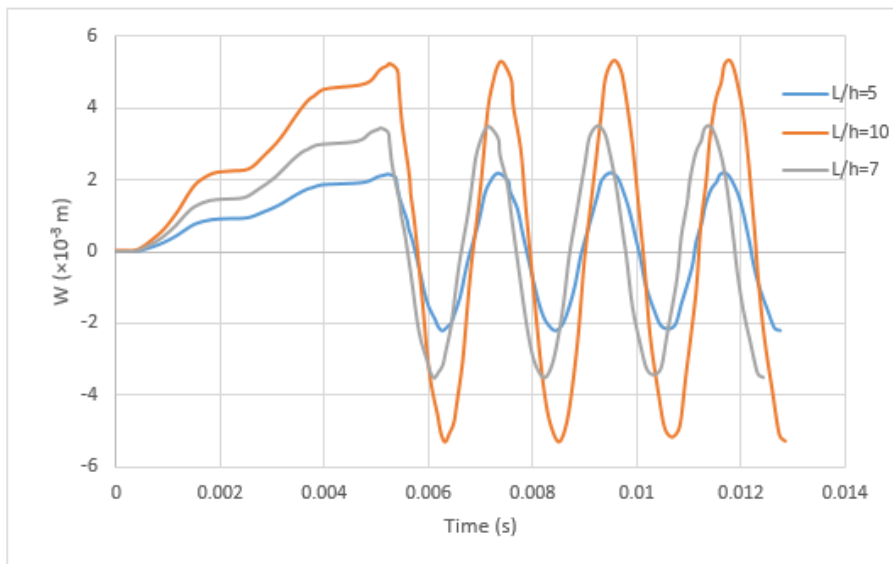
Fig 3. The influences of various aspect ratio on time history of midpoint transverse displacement of the simply supported 3D printed sandwich beam (TD1,e0=0.5, Re-entrant auxetic cell, l/d=1, $\psi = 60^0$,e₀=0.5)
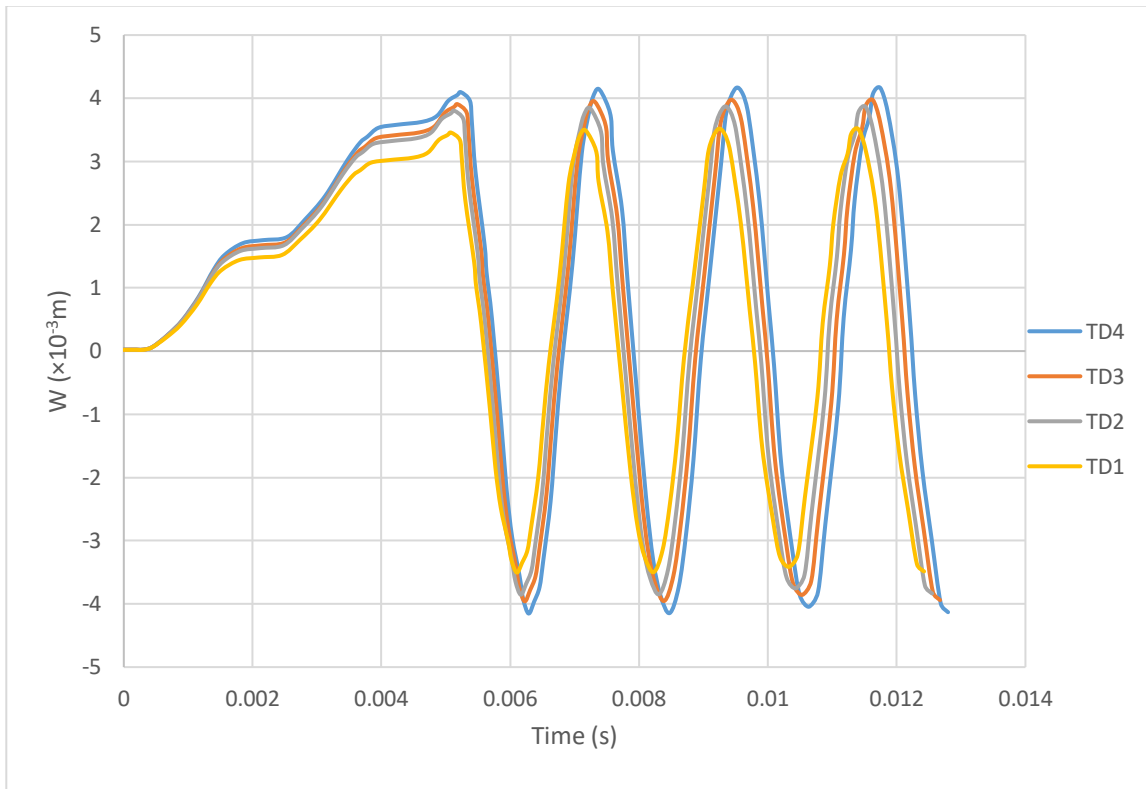
Fig 4. The influences of various thickness patterns on time history of midpoint transverse displacement of the simply supported 3D printed sandwich beam (e0=0.5, Re-entrant auxetic cell, l/d=1, $\psi = 60^0$,e$_0$=0.5,L/h=5)
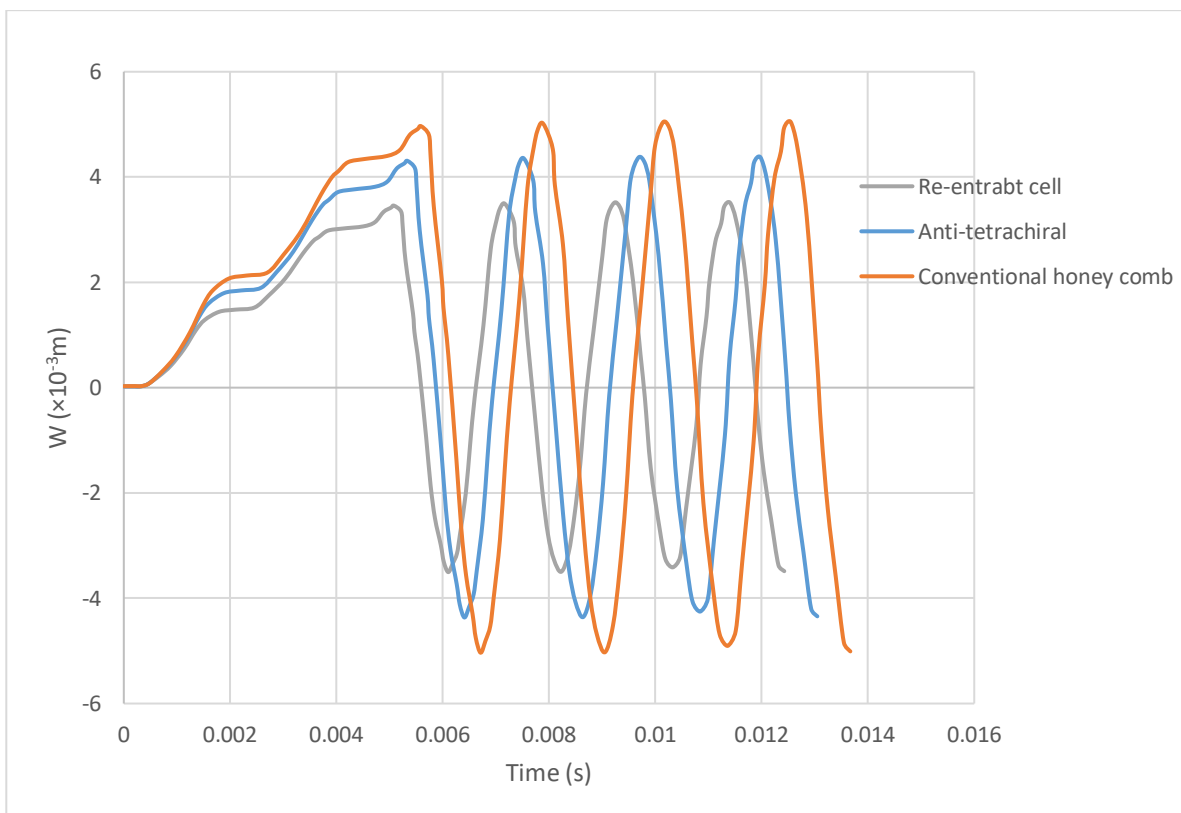

Fig 5. The influences of various core cells   on time history of midpoint transverse displacement of the simply

supported 3D printed sandwich beam (e0=0.5, h/l=1,L/r=3, TD2, l/d=1, $\psi = 60^0$,e$_0$=0.5,L/h=5)
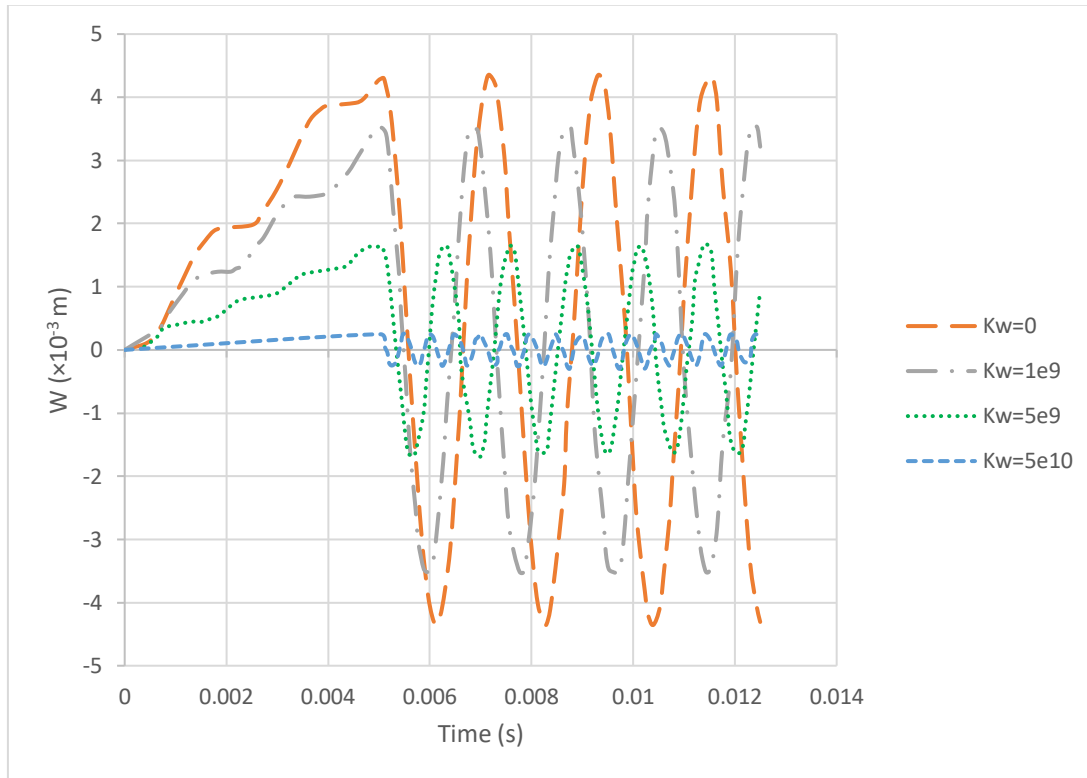

Fig6. The effect of elastic coefficient of foundation on time history of midpoint transverse displacement of simply supported 3D printed sandwich beam (TD1,Re-entrant auxetic cell, l/d=1, $\psi = 60^0$,L/h=5)
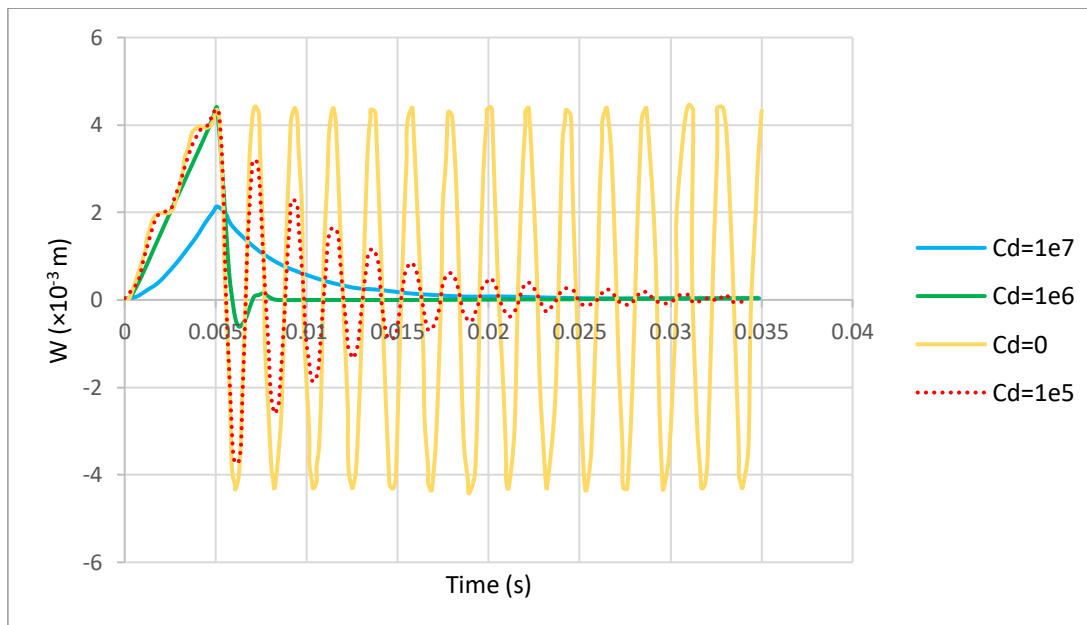

Fig7. The effect of damping coefficient of foundation on time history of midpoint transverse displacement of simply supported 3D printed sandwich beam (TD1,Re-entrant auxetic cell, l/d=1, $\psi = 60^0$,L/h=5)

1) In symmetric thickness distribution (A), anti-tetrachiral auxetic cell has the most amounts of natural frequencies while in another one the most amounts of natural frequencies belong to Re-entrant auxetic cell.
2) The minimum amounts of natural frequencies of is related to conventional honeycomb cell with uniform thickness distribution.
3) The maximum difference between natural frequencies of various cells is at least approximately 70%.
4) By increasing the angle of Re-entrant auxetic cells and decreasing the angle of conventional honeycomb cells, the natural frequencies increase.
5) In Re-entrant auxetic cell and conventional honeycomb, the maximum difference between various thickness distribution is lower than 20%.
6) In anti-tetrachiral auxetic cell the maximum difference between various thickness distribution is at least approximately 36%.
7) By increasing the thickness coefficient and aspect ratio the amounts of natural frequencies decrease.
8) By increasing the thickness coefficient, the amplitude vibration increase.
9) By increasing damping of the foundation, amplitude of vibration decreases and vibration of beam can be seen in three situations such as under-damped, critically-damped and over-damped.
10) By increasing the elastic coefficient of the foundation, amplitude of transverse displacement decrease significantly.

Appendix:

$$N_{4i-3} = 1 - \frac{x}{l}$$

$$N_{4j-3} = \frac{x}{l}$$

$$N_{4i} = 1 - \frac{x}{l}$$

$$N_{4j} = \frac{x}{l}$$

$$N_{4i-2} = 1 - \frac{3x^2}{l^2} + \frac{2x^3}{l^3}$$

$$N_{4i-2} = 1 - \frac{3x^2}{l^2} + \frac{2x^3}{l^3}$$ $(A.1)$

$$N_{4i-1} = x - \frac{2x^2}{l} + \frac{x^3}{l^2}$$

$$N_{4j-2} = \frac{3x^2}{l^2} - \frac{2x^3}{l^3}$$

$$N_{4j-1} = -\frac{x^2}{l} + \frac{x^3}{l^2}$$

$$[N]$$
$$= \begin{bmatrix} N_{4i-3} & 0 & 0 & 0 & N_{4j-3} & 0 & 0 & 0 \\ 0 & N_{4i-2} & N_{4i-1} & 0 & 0 & N_{4j-2} & N_{4j-1} & 0 \\ 0 & \frac{\partial N_{4i-2}}{\partial x} & \frac{\partial N_{4i-1}}{\partial x} & 0 & 0 & \frac{\partial N_{4j-2}}{\partial x} & \frac{\partial N_{4j-1}}{\partial x} & 0 \\ 0 & 0 & 0 & N_{4i} & 0 & 0 & 0 & N_{4j} \end{bmatrix} \quad (A.2)$$

$$[B]$$

$$= \begin{bmatrix} \dfrac{\partial N_{4i-3}}{\partial x} & 0 & 0 & 0 & \dfrac{\partial N_{4j-3}}{\partial x} & 0 & 0 & 0 \\[2mm] 0 & 0 & 0 & \dfrac{\partial N_{4i}}{\partial x} & 0 & 0 & 0 & \dfrac{\partial N_{4j}}{\partial x} \\[2mm] 0 & \dfrac{\partial^2 N_{4i-2}}{\partial x^2} & \dfrac{\partial^2 N_{4i-1}}{\partial x^2} & 0 & 0 & \dfrac{\partial^2 N_{4j-2}}{\partial x^2} & \dfrac{\partial^2 N_{4j-1}}{\partial x^2} & 0 \\[2mm] 0 & \dfrac{\partial N_{4i-2}}{\partial x} & \dfrac{\partial N_{4i-1}}{\partial x} & N_{4i} & 0 & \dfrac{\partial N_{4j-2}}{\partial x} & \dfrac{\partial N_{4j-1}}{\partial x} & N_{4j} \end{bmatrix} \qquad (A.3)$$

$$[\bar{N}] = \begin{bmatrix} 0 & 0 & 0 & 0 & 0 & 0 & 0 & 0 \\ 0 & N_{4i-2} & N_{4i-1} & 0 & 0 & N_{4j-2} & N_{4j-1} & 0 \\ 0 & 0 & 0 & 0 & 0 & 0 & 0 & 0 \\ 0 & 0 & 0 & 0 & 0 & 0 & 0 & 0 \end{bmatrix} \qquad (A.4)$$

References

[1]   M. Gunasegeran, P. Edwin Sudhagar, Free and forced vibration analysis of 3D printed bioinspired sandwich beam using HSDT: Numerical and experimental study, *Polymer Composites,* Vol. 43, No. 6, pp. 3659-3677, 2022.

[2]   Z. Guo, G. Hu, J. Jiang, L. Yu, X. Li, J. Liang, Theoretical and experimental study of the vibration dynamics of a 3D-printed sandwich beam with an hourglass lattice truss core, *Frontiers in Mechanical Engineering,* Vol. 7, pp. 651998, 2021.

[3]   R. Rajpal, K. Lijesh, K. Gangadharan, Experimental investigation of 3D-printed polymer-based MR sandwich beam under discretized magnetic field, *Journal of the Brazilian Society of Mechanical Sciences and Engineering,* Vol. 40, pp. 1-11, 2018.

[4]   S. Ghannadpour, M. Mahmoudi, K. H. Nedjad, Structural behavior of 3D-printed sandwich beams with strut-based lattice core: Experimental and numerical study, *Composite Structures,* Vol. 281, pp. 115113, 2022.

[5]   S. Li, Z. Liu, V. Shim, Y. Guo, Z. Sun, X. Li, Z. Wang, In-plane compression of 3D-printed self-similar hierarchical honeycombs–static and dynamic analysis, *Thin-Walled Structures,* Vol. 157, pp. 106990, 2020.

[6]   Y. Solyaev, A. Babaytsev, A. Ustenko, A. Ripetskiy, A. Volkov, Static and dynamic response of sandwich beams with lattice and pantographic cores, *Journal of Sandwich Structures & Materials,* Vol. 24, No. 2, pp. 1076-1098, 2022.

[7]   K. Essassi, J.-L. Rebiere, A. E. Mahi, M. A. B. Souf, A. Bouguecha, M. Haddar, Experimental and numerical analysis of the dynamic behavior of a bio-based sandwich with an auxetic core, *Journal of Sandwich Structures & Materials,* Vol. 23, No. 3, pp. 1058-1077, 2021.

[8]   U. Sharif, B. Sun, I. Tariq, D. S. Ibrahim, O. O. Adewale, A. Zafar, Static and modal analysis of sandwich beam structure with magnetorheological honeycomb core, in *Proceeding of,* IEEE, pp. 19-23.

[9]   A. Ingrole, A. Hao, R. Liang, Design and modeling of auxetic and hybrid honeycomb structures for in-plane property enhancement, *Materials & Design,* Vol. 117, pp. 72-83, 2017.

[10]   M. Dryzek, W. Cecot, M. Tekieli, Experimental and multiscale computational static and dynamic study of 3D printed elements with mesostructure, *Finite Elements in Analysis and Design,* Vol. 215, pp. 103876, 2023.

[11]   Z. Wu, J. Wu, F. Lu, C. Zhang, Z. Liu, Y. Zhu, Free vibration analysis and multi-objective optimization of lattice sandwich beams, *Mechanics of Advanced Materials and Structures*, pp. 1-14, 2023.

[12]   U. Sharif, L. Chen, B. Sun, D. S. Ibrahim, O. O. Adewale, N. Tariq, An experimental study on dynamic behaviour of a sandwich beam with 3D printed hexagonal honeycomb core filled with magnetorheological elastomer (MRE), *Smart Materials and Structures,* Vol. 31, No. 5, pp. 055004, 2022.

[13] M. Refat, E. Zappino, A. Racionero Sanchez-Majano, A. Pagani, Dynamic characterization of 3D printed lightweight structures, *Advances in Aircraft and Spacecraft Science,* Vol. 9, No. 4, pp. 301-318, 2022.

[14] A. Hamrouni, J.-L. Rebiere, A. El Mahi, M. Beyaoui, M. Haddar, Experimental and finite element analyses of a 3D printed sandwich with an auxetic or non-auxetic core, *Journal of Sandwich Structures & Materials*, pp. 10996362231151454, 2023.

[15] V. Kallannavar, S. Kattimani, Effect of temperature and porosity on free vibration characteristics of a doubly-curved skew laminated sandwich composite structures with 3D printed PLA core, *Thin-Walled Structures,* Vol. 182, pp. 110263, 2023.

[16] M. Hedayatian, A. Daneshmehr, G. Liaghat, The efficiency of auxetic cores in sandwich beams subjected to low-velocity impact, *International Journal of Applied Mechanics,* Vol. 12, No. 06, pp. 2050061, 2020.

[17] J. Gan, F. Li, K. Li, E. Li, B. Li, Dynamic failure of 3D printed negative-stiffness meta-sandwich structures under repeated impact loadings, *Composites Science and Technology*, pp. 109928, 2023.

[18] A. Hamrouni, J.-L. Rebiere, A. El Mahi, M. Beyaoui, M. Haddar, Experimental and numerical investigation of the static behavior of a 3D printed bio-based anti-trichiral sandwich, *Journal of Composite Materials,* Vol. 57, No. 13, pp. 2161-2178, 2023.

[19] M. Eryildiz, Experimental investigation and simulation of 3D printed sandwich structures with novel core topologies under bending loads, *International Polymer Processing*, No. 0, 2023.

[20] X. Zhang, Y. Wang, M. Su, Experimental, numerical and analytical study to develop a design method for bending and shear resistances of 3D printed beetle elytron inspired sandwich plate (beetle elytron plate), *Thin-Walled Structures,* Vol. 183, pp. 110371, 2023.

[21] Y. Jiang, Y. Li, 3D printed auxetic mechanical metamaterial with chiral cells and re-entrant cores, *Scientific reports,* Vol. 8, No. 1, pp. 1-11, 2018.

[22] M. Najafi, H. Ahmadi, G. Liaghat, Investigation on the flexural properties of sandwich beams with auxetic core, *Journal of the Brazilian Society of Mechanical Sciences and Engineering,* Vol. 44, No. 2, pp. 61, 2022.

[23] M. Najafi, H. Ahmadi, G. Liaghat, Evaluation of the mechanical properties of fully integrated 3D printed polymeric sandwich structures with auxetic cores: experimental and numerical assessment, *The International Journal of Advanced Manufacturing Technology,* Vol. 122, No. 9-10, pp. 4079-4098, 2022.

[24] X. Zhang, H. Zhou, W. Shi, F. Zeng, H. Zeng, G. Chen, Vibration tests of 3D printed satellite structure made of lattice sandwich panels, *AIAA Journal,* Vol. 56, No. 10, pp. 4213-4217, 2018.

[25] P. Boron, J. Chelmecki, J. M. Dulinska, N. Jurkowska, B. Ratajewicz, P. Stecz, T. Tatara, On the Possibility of Using 3D Printed Polymer Models for Modal Tests on Shaking Tables: Linking Material Properties Investigations, Field Experiments, Shaking Table Tests, and FEM Modeling, *Materials,* Vol. 16, No. 4, pp. 1471, 2023.

[26] Y. Chai, S. Du, F. Li, C. Zhang, Vibration characteristics of simply supported pyramidal lattice sandwich plates on elastic foundation: Theory and experiments, *Thin-Walled Structures,* Vol. 166, pp. 108116, 2021.

[27] C. Li, H.-S. Shen, H. Wang, Z. Yu, Large amplitude vibration of sandwich plates with functionally graded auxetic 3D lattice core, *International Journal of Mechanical Sciences,* Vol. 174, pp. 105472, 2020.

[28] R. Wang, J. Shang, X. Li, Z. Luo, W. Wu, Vibration and damping characteristics of 3D printed Kagome lattice with viscoelastic material filling, *Scientific reports,* Vol. 8, No. 1, pp. 1-13, 2018.

[29] M. H. Zamani, M. Heidari-Rarani, K. Torabi, A novel graded auxetic honeycomb core model for sandwich structures with increasing natural frequencies, *Journal of Sandwich Structures & Materials,* Vol. 24, No. 2, pp. 1313-1339, 2022.

[30] L. Meng, X. Qiu, T. Gao, Z. Li, W. Zhang, An inverse approach to the accurate modelling of 3D-printed sandwich panels with lattice core using beams of variable cross-section, *Composite Structures,* Vol. 247, pp. 112363, 2020.

[31] M. F. Ashby, L. J. Gibson, Cellular solids: structure and properties, *Press Syndicate of the University of Cambridge, Cambridge, UK*, pp. 175-231, 1997.

[32] F. Kiarasi, M. Babaei, P. Sarvi, K. Asemi, M. Hosseini, M. Omidi Bidgoli, A review on functionally graded porous structures reinforced by graphene platelets, *Journal of Computational Applied Mechanics,* Vol. 52, No. 4, pp. 731-750, 2021.

[33] M. Babaei, F. Kiarasi, K. Asemi, M. Hosseini, Functionally graded saturated porous structures: A review, *Journal of Computational Applied Mechanics,* Vol. 53, No. 2, pp. 297-308, 2022.

[34] M. Khatoonabadi, M. Jafari, F. Kiarasi, M. Hosseini, M. Babaei, K. Asemi, Shear buckling response of FG porous annular sector plate reinforced by graphene platelet subjected to different shear loads, *Journal of Computational Applied Mechanics,* Vol. 54, No. 1, pp. 68-86, 2023.

[35]   F. Kiarasi, M. Babaei, S. Mollaei, M. Mohammadi, K. Asemi, Free vibration analysis of FG porous joined truncated conical-cylindrical shell reinforced by graphene platelets, *Advances in nano research,* Vol. 11, No. 4, pp. 361, 2021.

[36]   M. Babaei, K. Asemi, P. Safarpour, Buckling and static analyses of functionally graded saturated porous thick beam resting on elastic foundation based on higher order beam theory, *Iranian Journal of Mechanical Engineering Transactions of the ISME,* Vol. 20, No. 1, pp. 94-112, 2019.

[37]   S. Z. Gebrehiwot, L. Espinosa Leal, J. Eickhoff, L. Rechenberg, The influence of stiffener geometry on flexural properties of 3D printed polylactic acid (PLA) beams, *Progress in additive manufacturing,* Vol. 6, pp. 71-81, 2021.

[38]   S. Chahardoli, Flexural behavior of sandwich panels with 3D printed cellular cores and aluminum face sheets under quasi-static loading, *Journal of Sandwich Structures & Materials,* Vol. 25, No. 2, pp. 232-250, 2023.